Journal of Information Systems Engineering and Management
2025, 10(13s)
e-ISSN: 2468-4376
https://www.jisem-journal.com/

Research Article

Numerical Evaluation of Seismic Performance of Concrete Tunnels Considering Concrete Liner Parameters

Walaa Hussein Kamil1, Hadi Bahadori2
1College of Engineering,Urmia University,Urmia (Iran),email walaahk20232023@gmail.com
2Department of Civil Engineering,Urmia University,Urmia (Iran),email h.bahadori@urmia.ac.ir

ARTICLE INFO

Received: 28 Nov 2024
Revised: 10 Jan 2025
Accepted: 31 Jan 2025

ABSTRACT

The tunnel form concrete system is a new industrial construction method to facilitate construction management and reduce construction time and related financial risks. Unlike conventional framed structures, this system does not have columns and beams. However, the wall and slab elements resist lateral and gravity loads. One of the most important factors producing axial forces, shear forces, and bending moments in concrete tunnels is earthquakes. Tunnels are inherently stronger than structures on the ground. Earthquake damage in different regions of the world has highlighted the importance of creating dynamic loads in the design of concrete tunnels. This study aims to numerically evaluate the seismic performance of concrete tunnels considering soil-structure interaction. The main innovation of this research is the comparison of numerical results with analytical methods and results. According to studies, although analytical methods may provide responses, often the responses are too long and difficult or it is impossible to measure the dynamic load in tunnels accurately. As a result, numerical methods are used to investigate the seismic performance of concrete tunnels by considering soil-structure interaction. To implement numerical methods, FLAC3D software is used to model the behavior of structures built in rock and soil. The main advantage of numerical methods over analytical methods is the continuous concrete liner. According to the results, increasing the bending moment deformation modulus leads to a decrease in the axial force in the concrete tunnel liner. Subsequently, strengthening the thickness of the tunnel concrete liner leads to an increase in the bending moment. Finally, increasing the number of concrete liner pieces leads to a decrease in the maximum axial force and shear force.

Keywords: Concrete tunnel, seismic performance, dynamic load analysis, numerical modeling.

INTRODUCTION

Given the increasing advances in tunnels and the importance of their role in realizing the transportation network of cities and towns, analyzing the dynamic response of tunnels to dynamic loads is vital. Analysis of critical loads is possible in both natural and unnatural forms. Earthquake loads are one of the most important natural loads. Regarding engineering, the importance of earthquakes stems from their effects on various structures, especially underground structures. For the design of structures under earthquakes, it is vital to estimate the effect of seismic waves on the structure accurately and to gain a proper understanding of it. There are various theories about earthquake mechanisms. However, the causes of earthquakes are closely related to the changes in the earth's subsurface.

In the past twenty years, many studies have been conducted focusing on various aspects of tunnel construction. The high strength and good seismic performance of these systems have been proven. Balkaya and Kalkan [1] performed a modal and non-tunnel static analysis on a tunnel-form material model to evaluate the effect of cavity and wall deflection on the load transfer mechanism. Based on the results, the researchers proposed corrections and feedback correlations for the time estimation of tunnel systems. Kalkan and Yüksel [2] analyzed the effects of design considerations and different

construction methods on the strengths and weaknesses of tunnel structures. Yüksel [3] proposed a deep connection cavity for the tunnel building and evaluated the performance of buildings with such a connection using two-dimensional static and dynamic analysis. Beheshti-Aval et al. [4] investigated the seismic performance of concrete tunnel structures under near- and far-field earthquake excitations using dynamic deformation analysis. Mohsenian and Mortezaei [5] analyzed the effect of random rotation on the reliability of tunnel-shaped structures using dynamic analysis and performance-based design methods. Mohsenian et al. [6] studied the effect of mass and stiffness complexity on the seismic performance of structural systems. Mohsenian et al. [7] showed that eccentricity up to 20% of the design does not significantly affect the seismic performance of concrete tunnel structures. Mohsenian and Mortezaei [8] proposed an appropriate drift ratio as a damage criterion for the performance-based design of tunnel structures after comparing local and global damage metrics. Mohsenian and Nikkhoo [9] and Mohsenian et al. [10, 11] discussed the results of the distribution of time constraints, scheduling, height, and seismic vulnerability of tunnel structures. In another study, Mohsenian et al. [12] investigated the effect of soil-structure interaction on the seismic performance of tunnel-shaped structures. Mortezaei and Mohsenian [13] included eigenvalue, density, nonlinear time history, and fragility in the process of evaluating the effect of shear rate distortion, strength, and stiffness on the seismic reliability of the tunnel model.

Faisal et al. [15] investigated the design of the floor of a multi-story concrete structure under seismic excitation. Song et al. [16] analyzed the effect of frequency content and risk duration on the collapse of damaged buildings and large shocks. The researchers believe that using granularity as a failure predictor does not provide reliable results for failure risk assessment. Ruiz-García et al. [17] conducted a study on four sections from the lowest to the highest elevation of a concrete structure to determine the effect of soft soil on the performance of structures during an earthquake. Li et al. [18] evaluated the effect of the initial record, fault type, and different nature of dimensional displacement and structural damage during cyclic loading on the collapse capacity of the structure. Han et al. [19] presented a new method for comparing the seismic performance of unreinforced concrete structures under earthquakes.

Trevlopoulos and Guéguen [20] introduced a performance-based method for modeling the time-varying fragility of strong structures under earthquakes using fragility analysis and Markov chain. Similarly, Wen et al. [21] proposed an engineering design principle (EDP)-based method to evaluate the fragility of structures under an initial collapse process and demonstrated its effectiveness by analyzing a 5-story structure under continuous seismic activity. Ruiz-Garcia and Aguilar [22] evaluated a 4-story steel building to analyze the flexural effect on the aftershock response of steel structures and showed the effect of stiffness in such sources.

Oyguc et al. [23] developed a 3D model of unreinforced concrete to investigate the effect of multiple excitations on the seismic behavior of such systems. Veismoradi et al. [24] investigated the aftershock failure capacity of reinforced concrete frames through an incremental strength and fragility analysis. Ruiz-García et al. [25] investigated the performance of reinforced concrete frames on soft ground and included them in an inverse shear system. Liu et al. [26] analyzed the effect of critical shape on different types of damage caused by mainshocks on the fragility of four-story reinforced concrete buildings.

Owen and Scholl [27] believe that the motion of an underground structure during an earthquake can be approximated by an elastic strain related to the deformation of the ground. According to Penzien [28] and Hashash et al. [29], except for fault-cut tunnels, the most influential component of the behavior of the tunnel liner under seismic loads is the change in the tunnel cross-section caused by shear wave propagation. Hashash et al. analyzed the differences in the methods used by Wang, Penzien, and Wu and tried to better understand these differences and their origin in the context of similar concepts of numerical models. The comparison clearly shows that Wang's solution provides a more accurate estimate of the support liner in unstable conditions. Also, Penzien's method should not be used under any circumstances. These differences were also reported by Park et al. and Bazaz and Besharat [30]. Wang [31] introduced the first closed-loop solution for determining the forces

generated in tunnel supports under seismic loads. Specific relations for determining the normal force and the bending moment under no-slip conditions have also been presented. Kouretzis et al. [32] proposed another relation to determine the maximum bending moment under no-slip conditions to improve Wang's method.

With the increasing progress of technology and computers in the last decade, the use of numerical methods and two-dimensional and three-dimensional models for analyzing the behavior of tunnels under earthquake loads has increased. Often, the static load is equal to the dynamic load and imposes less structural resistance on the insulation. The safety effect of tunnels under seismic loads has also been evaluated by Torcato et al. [33]. In all the studies mentioned, a continuous liner has been considered. Pakbaz and Yareevand [34] also performed numerical simulation and two-dimensional analysis using CA2 software to investigate the effect of seismic loading in a square-centered and circular tunnel on elastoplastic behavior. To show the differences and similarities between the numerical method and closed-form solutions, the simulation results were compared with the closed-form solution.

Over the past few decades, the increase in the world population and the increasing need to move to urban areas have led to an increase in the use of tunnels. The tunnel maintenance method is based on designed components consisting of rings installed next to each other. The rings rotate together on the sides of the body and form the tunnel liner. The design of such a system must meet the requirements of stability, durability, and cost of the device. To fulfill such requirements, the forces that the barrier will withstand during its working life must be determined. Earthquakes are one of the factors that cause axial and shear forces as well as bending moments in tunnels. Although tunnels are safer than ground structures, earthquake damage to tunnels has highlighted the urgent need for the design of underground structures.

Several methods with various modifications have been proposed to assess the stability and behavior of these structures against vertical loads and forces, such as closed-loop investigation methods, quantitative methods, numerical methods, and physical experiments. Precast concrete components are used for the safety and security of excavated tunnels. Many researchers have investigated the behavior of these concrete components against vertical loads caused by heavy loads. However, the seismic behavior of support systems has not been studied much despite its increasing importance. The main objective of this study is to numerically analyze the seismic performance of tunnels by considering the relationship between the structure and the soil.

Methodology

The dynamic response of different components based on the change of axial strength, shear strength, and bending moment is studied by examining the effect of parameters such as deformation modulus, adhesion, number of internal components, tensile strength, and thickness of the support liner. Also, the effect of the tunnel environment on the response performance of different tunnel sections is investigated. In this regard, numerical analyses were carried out in different soil environments based on the finite difference method using FLAC3D software.

Regarding geometric considerations, the ring is a part of a cylinder that is realized in parallel (vertical ring) or non-parallel (trapezoidal ring), as shown in Figure (1) [35]. The length of the ring is between 0.6 and 2 m. At the same time, the value of this parameter in road tunnels is usually between 1.2 and 1.7 m due to the presence of corners and a small radius. Also, the number of pieces can be directly related to the TBM pressure system especially the number of pressure jacks. A general rule is to avoid including pressure insoles on the edges of different parts. Also, the minimum number of insoles is equal to the connection between the surrounding pieces. This means that there is a specific constraint between each component, the ring material, and the number of insoles [35].

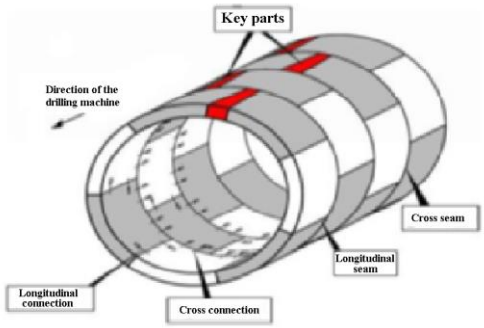

Figure 1: Schematic of four concrete rings [36]

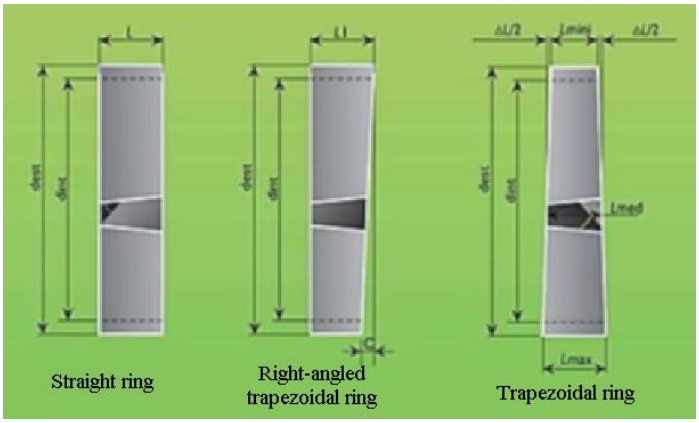

Figure 2: A side view of different types of concrete rings [35]

For the numerical modeling of concrete rings in FLAC3D software and also the analytical methods used, namely Wang, Penzein, and Bobet methods, the parameters in Table (1) were used.

Table 1: Parameters

Parameter	Value	Unit
Modulus of elasticity	25×10^9	Pa
Poisson's ratio	0.15	-
Thickness	0.3, 0.4, and 0.5	M
Width	1.4	M
Density	2200	kg/m^3
Number of concrete pieces	1, 3, 5, and 7	-
Ring radius	3	m

The displacement-time plot shown in Figure 3 was obtained by using the system excitation under gravitational acceleration. Based on this, the time of environment generation can be determined. The value of this parameter for the models involved in this study is equal to 3.5 Hz.

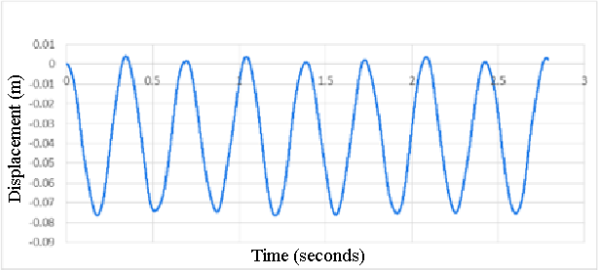

Figure 3: Displacement-time plot using the system excitation under gravity acceleration

Results

The parameters related to the concrete liner including the diameter and number of concrete components are investigated in the following section.

Diameter of the support system

In the models used, the diameter of the support system is changed to 0.3, 0.4, and 0.5 m and the results are presented. In Figures (4), (5), and (6), the values of bending moment, axial force, and tensile stress are shown separately based on the increase in the diameter of the support system and the soil type. The results obtained for the maximum bending moment, axial resistance, and maximum resistance in different environments for different sizes of material liners are presented in Table (2).

Table 2: Results obtained for bending moment, axial force, and maximum shear force in different environments containing the tunnel for a continuous concrete liner (n=1)

	Parameter	GW-Dense	SP-Dense	GM-Dense	GW-Loose	SP-Loose	GM-Loose
	Modulus of elasticity	$3/2 \times 10^7$	8×10^7	3×10^7	3×10^7	1×10^7	7×10^6
	Internal friction angle	40	39	40	33	30	30
30 cm	bending moment)Nm/m(	$3/02 \times 10^4$	$1/22 \times 10^5$	$1/73 \times 10^5$	$1/69 \times 10^5$	$4/05 \times 10^5$	$4/33 \times 10^5$
	Axial force (N)	$6/93 \times 10^5$	$4/44 \times 10^5$	$2/56 \times 10^5$	$2/83 \times 10^5$	$4/85 \times 10^5$	$4/92 \times 10^5$
	shear force (N)	$1/98 \times 10^5$	$1/96 \times 10^4$	$1/92 \times 10^4$	$1/85 \times 10^4$	$8/44 \times 10^3$	$7/87 \times 10^3$
40 cm	Bending moment (Nm/m)	$1/16 \times 10^4$	$8/94 \times 10^4$	$1/21 \times 10^5$	$1/23 \times 10^5$	$3/65 \times 10^5$	$3/99 \times 10^5$
	Axial force (N)	$7/18 \times 10^5$	$4/74 \times 10^5$	$2/59 \times 10^5$	$2/58 \times 10^5$	$5/00 \times 10^5$	$5/13 \times 10^5$
	shear force (N)	$2/30 \times 10^4$	$2/20 \times 10^4$	$2/08 \times 10^4$	$2/09 \times 10^4$	$1/35 \times 10^4$	$1/11 \times 10^4$
50 cm	bending moment (Nm/m)	$9/03 \times 10^4$	$3/61 \times 10^5$	$3/64 \times 10^5$	$3/61 \times 10^5$	$5/37 \times 10^5$	$5/77 \times 10^5$
	Axial force (N)	$7/35 \times 10^5$	$5/08 \times 10^5$	$2/89 \times 10^5$	$2/88 \times 10^5$	$5/03 \times 10^5$	$5/40 \times 10^5$
	shear force (N)	$2/45 \times 10^4$	$2/23 \times 10^4$	$2/14 \times 10^4$	$2/12 \times 10^4$	$1/86 \times 10^4$	$1/37 \times 10^4$

According to the results, increasing the diameter of the support system significantly increases the bending moment. It also seems that increasing the diameter of the support system does not cause any change in the axial force and shear force.

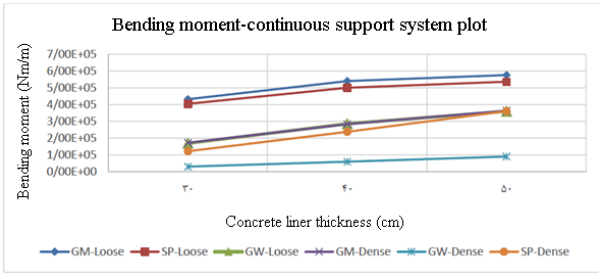

Figure 5: Bending moment-diameter of the support system (continuous support system) plot

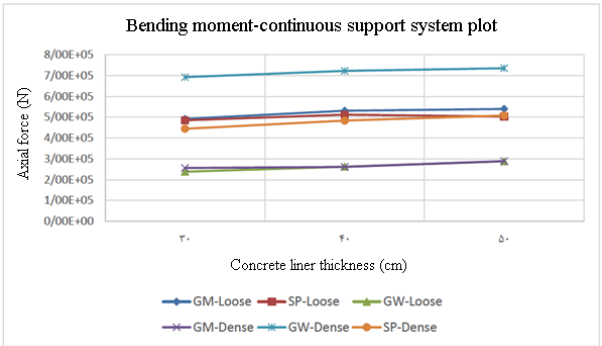

Figure 6: Axial force-diameter of the support system (continuous retention system) plot

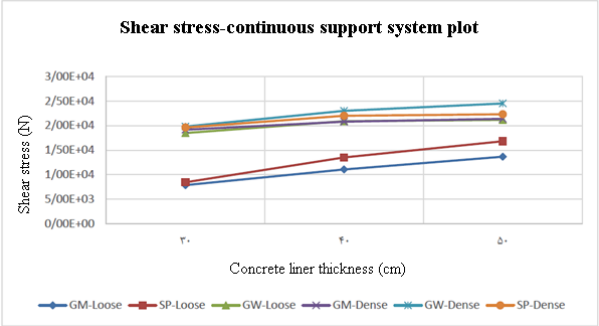

Figure 7: Shear force-diameter of support system (continuous retaining system) plot

Number of concrete components of support system

To analyze the effect of the number of prefabricated elements on the seismic response of the support process, the values of bending moment, axial force, and shear force were obtained for different types of continuous support processes. These experiments were conducted for various types of granular and dense soils and the results were extracted.

In general, increasing the number of different soil parts leads to a decrease in the values of bending moment, axial force, and stress in the support process. The maximum values of bending moment, axial resistance, and shear force for different numbers of parts and different liner diameters are shown in Tables (3), (4), and (5) respectively.

Table 3: Maximum values of bending moment for different numbers of concrete pieces and different diameters of concrete liner

$*_t$	$**_n$	GW-Dense	SP-Dense	GM-Dense	GW-Loose	SP-Loose	CH-Dense	CL-Dense
30	*1*	$3/02 \times 10^4$	$1/22 \times 10^5$	$1/73 \times 10^5$	$1/69 \times 10^5$	$4/05 \times 10^5$	$1/97 \times 10^5$	$1/15 \times 10^5$
	3	$1/23 \times 10^5$	$1/26 \times 10^5$	$1/85 \times 10^5$	$1/86 \times 10^5$	$1/92 \times 10^5$	$1/51 \times 10^5$	$1/49 \times 10^5$
	5	$1/16 \times 10^5$	$1/22 \times 10^5$	$1/13 \times 10^5$	$1/09 \times 10^5$	$1/06 \times 10^5$	$9/46 \times 10^4$	$1/48 \times 10^5$
	7	$4/05 \times 10^4$	$4/32 \times 10^4$	$3/92 \times 10^4$	$3/76 \times 10^4$	$5/65 \times 10^4$	$5/23 \times 10^4$	$4/28 \times 10^4$
40	*1*	$5/96 \times 10^4$	$2/38 \times 10^5$	$2/84 \times 10^5$	$2/86 \times 10^5$	$5/01 \times 10^5$	$3/27 \times 10^5$	$2/33 \times 10^5$
	3	$2/20 \times 10^5$	$2/36 \times 10^5$	$3/35 \times 10^5$	$3/36 \times 10^5$	$2/41 \times 10^5$	$2/32 \times 10^5$	$2/93 \times 10^5$
	5	$1/51 \times 10^5$	$2/77 \times 10^5$	$1/48 \times 10^5$	$1/41 \times 10^5$	$1/07 \times 10^5$	$1/25 \times 10^5$	$2/73 \times 10^5$
	7	$4/78 \times 10^4$	$5/66 \times 10^4$	$4/87 \times 10^4$	$4/44 \times 10^4$	$5/9 \times 10^4$	$6/37 \times 10^4$	$4/78 \times 10^4$
50	*1*	$9/03 \times 10^4$	$3/61 \times 10^5$	$3/61 \times 10^5$	$3/61 \times 10^5$	$5/87 \times 10^5$	$4/26 \times 10^5$	$3/65 \times 10^5$
	3	$2/86 \times 10^5$	$3/82 \times 10^5$	$4/72 \times 10^5$	$4/73 \times 10^5$	$2/40 \times 10^5$	$2/90 \times 10^5$	$4/69 \times 10^5$
	5	$1/64 \times 10^5$	$3/22 \times 10^5$	$1/46 \times 10^5$	$1/65 \times 10^5$	$1/08 \times 10^5$	$1/43 \times 10^5$	$3/87 \times 10^5$
	7	$4/65 \times 10^4$	$6/37 \times 10^4$	$4/43 \times 10^4$	$4/65 \times 10^4$	$6/16 \times 10^4$	$6/37 \times 10^4$	$6/29 \times 10^4$

* Diameter of concrete liner (cm)

** Number of concrete pieces

Table 4: Maximum axial force values for different numbers of concrete pieces and different diameters of concrete liner

$*_t$	$*_n$	GW-Dense	SP-Dense	GM-Dense	GW-Loose	SP-Loose	CH-Dense	CL-Dense
30	*1*	$6/93 \times 10^5$	$4/44 \times 10^5$	$2/56 \times 10^5$	$2/38 \times 10^5$	$4/85 \times 10^5$	$2/98 \times 10^5$	$7/23 \times 10^5$
	3	$3/19 \times 10^5$	$3/39 \times 10^5$	$3/22 \times 10^5$	$3/31 \times 10^5$	$3/02 \times 10^5$	$2/35 \times 10^5$	$4/18 \times 10^5$
	5	$2/49 \times 10^5$	$3/46 \times 10^5$	$2/54 \times 10^5$	$2/59 \times 10^5$	$2/82 \times 10^5$	$2/39 \times 10^5$	$4/19 \times 10^5$
	7	$1/98 \times 10^5$	$2/87 \times 10^5$	$1/99 \times 10^5$	$2/01 \times 10^5$	$2/95 \times 10^5$	$2/47 \times 10^5$	$2/78 \times 10^5$
40	*1*	$7/22 \times 10^5$	$4/84 \times 10^5$	$2/62 \times 10^5$	$2/62 \times 10^5$	$5/12 \times 10^5$	$3/02 \times 10^5$	$7/71 \times 10^5$
	3	$3/77 \times 10^5$	$4/12 \times 10^5$	$3/75 \times 10^5$	$3/68 \times 10^5$	$2/89 \times 10^5$	$2/61 \times 10^5$	$5/19 \times 10^5$
	5	$2/53 \times 10^5$	$3/99 \times 10^5$	$2/54 \times 10^5$	$2/54 \times 10^5$	$2/75 \times 10^5$	$2/48 \times 10^5$	$4/97 \times 10^5$
	7	$1/98 \times 10^5$	$2/90 \times 10^5$	$1/98 \times 10^5$	$1/98 \times 10^5$	$2/92 \times 10^5$	$2/12 \times 10^5$	$1/98 \times 10^5$
50	*1*	$7/35 \times 10^5$	$5/08 \times 10^5$	$2/87 \times 10^5$	$2/88 \times 10^5$	$5/03 \times 10^5$	$3/37 \times 10^5$	$7/39 \times 10^5$
	3	$4/07 \times 10^5$	$4/75 \times 10^5$	$4/04 \times 10^5$	$4/07 \times 10^5$	$2/84 \times 10^5$	$2/81 \times 10^5$	$6/00 \times 10^5$
	5	$2/53 \times 10^5$	$4/21 \times 10^5$	$2/58 \times 10^5$	$2/53 \times 10^5$	$2/69 \times 10^5$	$2/55 \times 10^5$	$5/32 \times 10^5$
	7	$1/99 \times 10^5$	$2/81 \times 10^5$	$1/94 \times 10^5$	$1/99 \times 10^5$	$2/91 \times 10^5$	$2/51 \times 10^5$	$2/73 \times 10^5$

* Diameter of concrete liner (cm)

** Number of concrete pieces

Table 5: Maximum shear force values for different numbers of concrete pieces and different diameters of concrete liner

$*_t$	$**_n$	GW-Dense	SP-Dense	GM-Dense	GW-Loose	SP-Loose	CH-Dense	CL-Dense
30	*1*	$1/15 \times 10^5$	$8/25 \times 10^4$	$1/92 \times 10^4$	$1/85 \times 10^4$	$8/44 \times 10^3$	$6/93 \times 10^1$	$3/54 \times 10^5$
	3	$3/11 \times 10^4$	$2/65 \times 10^4$	$3/09 \times 10^4$	$3/02 \times 10^4$	$1/08 \times 10^4$	$8/96 \times 10^3$	$2/62 \times 10^4$
	5	$2/50 \times 10^4$	$2/60 \times 10^4$	$2/43 \times 10^4$	$2/40 \times 10^4$	$3/94 \times 10^3$	$4/33 \times 10^3$	$2/65 \times 10^4$
	7	$2/07 \times 10^4$	$2/89 \times 10^4$	$1/97 \times 10^4$	$1/89 \times 10^4$	$1/02 \times 10^4$	$9/34 \times 10^3$	$2/85 \times 10^4$
	1	$9/86 \times 10^4$	$6/49 \times 10^4$	$2/07 \times 10^4$	$2/09 \times 10^4$	$1/35 \times 10^4$	$1/10 \times 10^2$	$4/15 \times 10^5$

40	3	4/07 $\times 10^4$	4/07 $\times 10^4$	4/07 $\times 10^4$	4/08 $\times 10^4$	1/37 $\times 10^4$	$1/56 \times 10^4$	4/24 $\times 10$
	5	2/89 $\times 10^4$	3/90 $\times 10^4$	2/77 $\times 10^4$	2/71 $\times 10^4$	3/98 $\times 10^3$	$5/49 \times 10^3$	4/14 $\times 10^4$
	7	2/25 $\times 10^4$	3/57 $\times 10^4$	2/13 $\times 10^4$	2/03 $\times 10^4$	1/02 $\times 10^4$	$1/15 \times 10^4$	2/25 $\times 10^4$
50	1	7/35 $\times 10^4$	5/08 $\times 10^4$	2/87 $\times 10^4$	2/88 $\times 10^4$	5/03 $\times 10^4$	$3/37 \times 10^2$	7/39 $\times 10^5$
	3	4/07 $\times 10^4$	4/75 $\times 10^4$	4/04 $\times 10^4$	4/07 $\times 10^4$	2/84 $\times 10^4$	$2/81 \times 10^4$	6/00 $\times 10^4$
	5	2/53 $\times 10^4$	4/21 $\times 10^4$	2/58 $\times 10^4$	2/53 $\times 10^4$	2/69 $\times 10^3$	$2/55 \times 10^3$	5/32 $\times 10^4$
	7	1/99 $\times 10^4$	2/81 $\times 10^4$	1/94 $\times 10^4$	1/99 $\times 10^4$	2/91 $\times 10^4$	$2/51 \times 10^4$	2/73 $\times 10^4$

* Diameter of concrete liner (cm)

** Number of concrete pieces

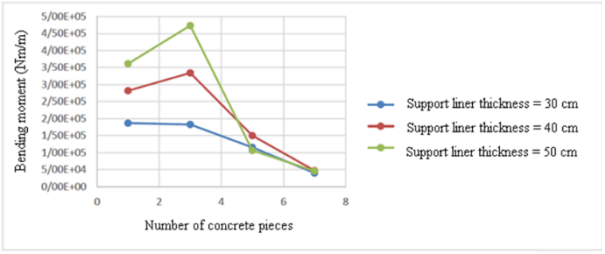

Figure 8: Bending moment-number of concrete pieces plot in dense GW soil

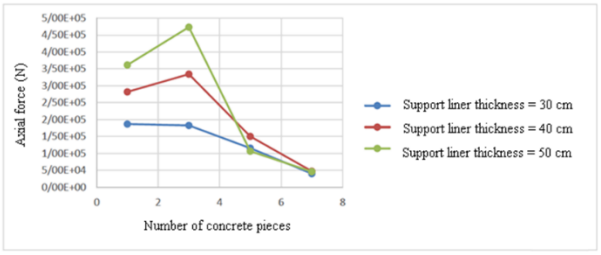

Figure 9: Axial force-number of concrete pieces plot in dense GW soil

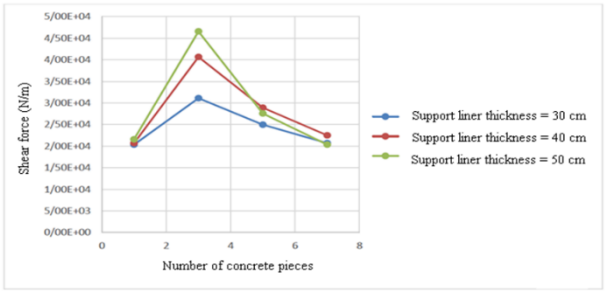

Figure 10: Shear stress-number of concrete pieces plot in dense GW soil

Plots of bending moment, axial force, and shear force are extracted for liners with three, five, and seven pieces with a diameter of 30 cm specific to dense GW soil samples. In addition, these plots are presented for compact liners with diameters of 40 and 50 cm and other types of soils including GW and non-GW limited soils.

As mentioned in the methodology section of the study, the maximum shear strength and bending moment are achieved at 45, 135, 225, and 315 degrees. The following figures present the bending moment, axial force, and shear force for different numbers of pieces.

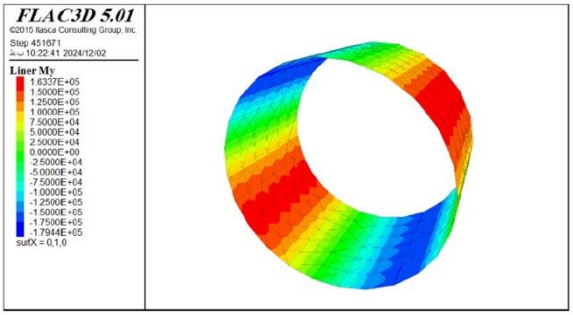

Figure 11: Bending moment plot of a continuous concrete liner with a diameter of 30 cm in dense GW soil

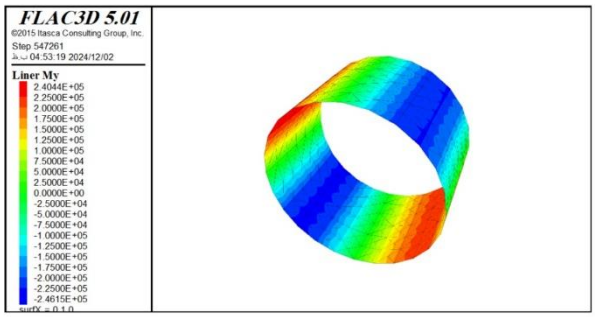

Figure 12: Bending moment plot of a continuous concrete liner with a diameter of 40 cm in dense GW soil

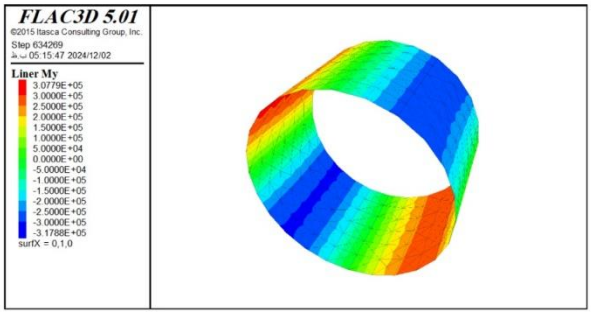

Figure 13: Bending moment plot of a continuous concrete liner with a diameter of 50 cm in dense GW soil

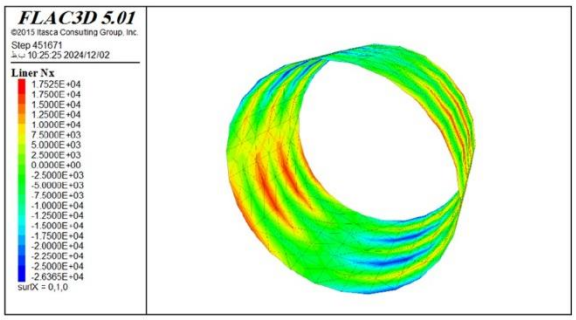

Figure 14: Axial force plot of a continuous concrete liner with a diameter of 30 cm in dense GW soil

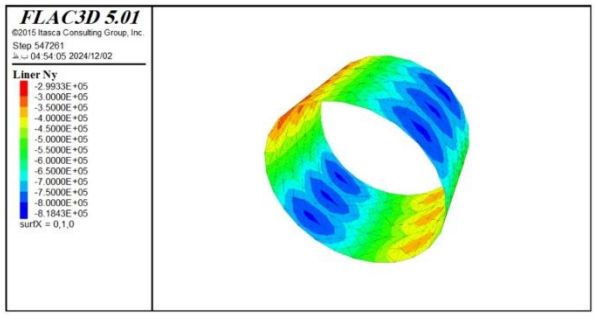

Figure 15: Axial force plot of a 40 cm diameter concrete liner in dense GW soil

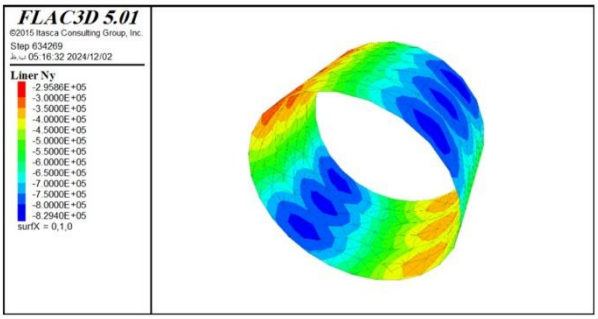

Figure 16: Axial force plot of a 50 cm diameter concrete liner in dense GW soil

Below, the plots of the variations of bending moment, axial force, and shear force regarding the number of concrete liner components are presented for the GW non-dense, SP dense, SP non-dense,

GM dense, CH dense, and CL dense soils. The following figures graphically show the effect of the number of bending elements on bending moment, axial force, and shear force. According to the plots, increasing the number of pieces has reduced the maximum parameters. This is because increasing the number of pieces leads to an increase in the number of longitudinal connections in the ring. Also, more displacement of the pieces increases the maximum value of these parameters.

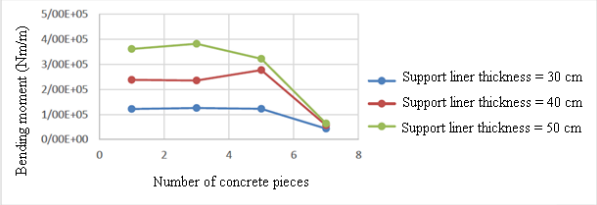

Figure 17: Bending moment-number of concrete pieces plot in dense SP soil

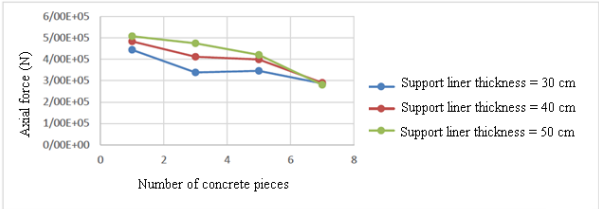

Figure 18: Axial force-number of concrete pieces plot in dense SP soil

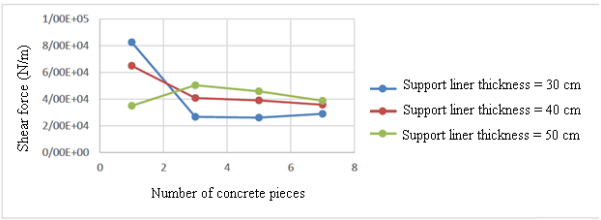

Figure 19: Shear stress-number of concrete pieces plot in dense SP soil

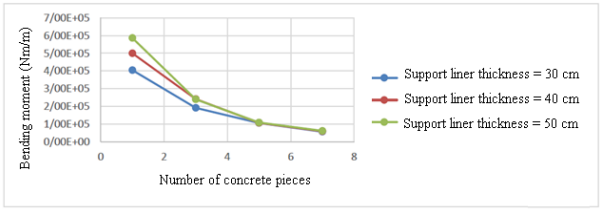

Figure 20: Bending moment-number of concrete pieces plot in non-dense SP soil

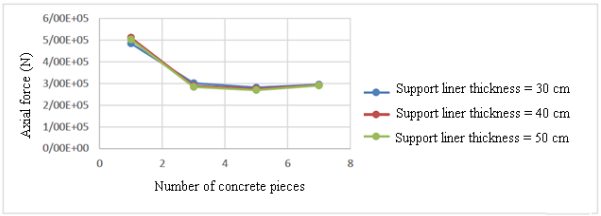

Figure 21: Axial force-number of concrete pieces plot in non-dense SP soil

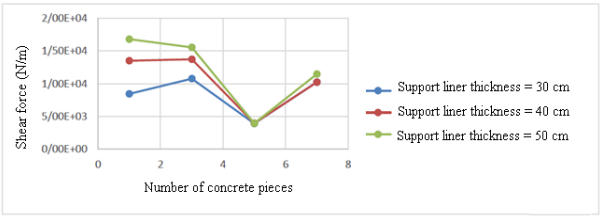

Figure 22: Shear stress-number of concrete pieces plot in non-dense SP soil

Conclusion

Analysis based on quantitative methods depends on many factors such as model size, mesh size, and power of the computer system used. In general, increasing the model size leads to an increase in the time of model execution and analysis. Also, increasing the number of meshes increases the time of model execution and analysis. Unlike analytical and closed methods, quantitative methods do not face many limitations. Tunnel lining and cohesive soil were included as prominent factors in the flexibility and effectiveness of the drainage system in this method. The cross-section of the support lining is circular. In general, increasing the deformation modulus reduces and increases the maximum axial force and resistance coefficient, respectively. Increasing the deformation modulus leads to a decrease in the maximum bending moment generated in the tunnel lining. Also, with increasing the diameter of the tunnel insulation, the bending moment increases significantly. It seems that increasing the diameter of the tunnel lining does not lead to a prominent change in the axial and shear forces generated in the lining.

The tunnels designed in this study were measured and analyzed as straight lines without gradients. Future research should evaluate the effect of curvature and gradient.

References

[1] C. Balkaya, E. Kalkan, Seismic vulnerability, behavior and design of tunnel form building structures, Eng. Struct. 26 (14) (2004) 2081-2099.

[2] E. Kalkan, S.B. Yüksel, Pros and cons of multistory RC tunnel-form (box-type) buildings, Struct. Des. Tall Special Build. 17 (3) (2008) 601–617.

[3] S.B. Yuksel, Slit-connected coupling beams for tunnel-form building structures, Struct. Des. Tall Special Build. 17 (3) (2008) 579-600.

[4] S.B. Beheshti-Aval, V. Mohsenian, H.S. Kouhestani, Seismic performance-based assessment of tunnel form building subjected to near-and far-fault ground motions, Asian J. Civil Eng. 19 (1) (2018) 79–92.

[5] V. Mohsenian, A. Mortezaei, Seismic reliability evaluation of tunnel form (box-type) RC structures under the accidental torsion, Struct. Concr. 19 (6) (2018) 1927-1938.

[6] V. Mohsenian, S. Rostamkalaee, A. Moghadam, Seismic reliability of tunnel form concrete buildings subjected to accidental torsion: a case study, 16th European Conference on Earthquake Engineering; Thessaloniki, Greece, 2018.

[7] V. Mohsenian, A. Nikkhoo, S. Rostamkalaee, A.S. Moghadam, F. Hejazi, The seismic performance of tunnel-form buildings with a non-uniform in-plan mass distribution, Structures 29 (2021) (2020) 993-1004.

[8] V. Mohsenian, A. Mortezaei, New proposed drift limit states for box-type structural systems considering local and global damage indices, Adv. Struct. Eng. 22 (15) (2019) 3352-3366.

[9] V. Mohsenian, A. Nikkhoo, A study on the effects of vertical mass irregularity on seismic performance of tunnel-form structural system, Adv. Concr. Construct. 7 (3) (2019) 131-141.

[10] V. Mohsenian, A. Nikkhoo, I. Hajirasouliha, Estimation of seismic response parameters and capacity of irregular tunnel-form buildings, Bull. Earthq. Eng. 17 (9) (2019) 5217-5239.

[11] V. Mohsenian, I. Hajirasouliha, S. Mariani, A. Nikkhoo, Seismic reliability assessment of RC tunnel-form structures with geometric irregularities using a combined system approach, Soil Dynamics and Earthquake Engineering, 2020, https://doi.org/10.1016/j.soildyn.2020.106356.

[12] V. Mohsenian, A. Nikkhoo, F. Hejazi, An investigation into the effect of soil- foundation interaction on the seismic performance of tunnel-form buildings, Soil Dynam. Earthq. Eng. 125 (2019) 2019, https://doi.org/10.1016/j.soildyn.2019. 105747.

[13] A. Mortezaei, V. Mohsenian, Reliability-based seismic assessment of multi-story box system buildings under the accidental torsion, J. Earthq. Eng. (2019) 1–24.

[14] J. Ruiz-García, J.C. Negrete-Manriquez, Evaluation of drift demands in existing steel frames under as-recorded far-field and near-fault mainshock-aftershock seismic sequences, Eng. Struct. 33 (2) (2011) 621-634.

[15] A. Faisal, T.A. Majid, G.D. Hatzigeorgiou, Investigation of story ductility demands of inelastic concrete frames subjected to repeated earthquakes, Soil Dynam. Earthq. Eng. 44 (2013) 42-53.

[16] R. Song, Y. Li, J.W. van de Lindt, Impact of earthquake ground motion characteristics on collapse risk of post-mainshock buildings considering aftershocks, Eng. Struct. 81 (2014) 349-361.

[17] J. Ruiz-García, M.V. Marín, A. Terán-Gilmore, Effect of seismic sequences in reinforced concrete frame buildings located in soft-soil sites, Soil Dynam. Earthq. Eng. 63 (2014) 56-68.

[18] Y. Li, R. Song, J.W. Van De Lindt, Collapse fragility of steel structures subjected to earthquake mainshock-aftershock sequences, J. Struct. Eng. 140 (12) (2014) 04014095.

[19] R. Han, Y. Li, J. van de Lindt, Impact of aftershocks and uncertainties on the seismic evaluation of non-ductile reinforced concrete frame buildings, Eng. Struct. 100 (2015) 149-163.

[20] K. Trevlopoulos, P. Guéguen, Period elongation-based framework for operative assessment of the variation of seismic vulnerability of reinforced concrete buildings during aftershock sequences, Soil Dynam. Earthq. Eng. 84 (2016) 224–237.

[21] W. Wen, C. Zhai, D. Ji, S. Li, L. Xie, Framework for the vulnerability assessment of structure under mainshock-aftershock sequences, Soil Dynam. Earthq. Eng. 101;(2017) 41-52

[22] J. Ruiz-Garcia, J.D. Aguilar, Influence of modeling assumptions and aftershock hazard level in the seismic response of post-mainshock steel framed buildings, Eng. Struct. 140 (2017) 437-446.

[23] R. Oyguc, C. Toros, A.E. Abdelnaby, Seismic behavior of irregular reinforced concrete structures under multiple earthquake excitations, Soil Dynam. Earthq. Eng. 104 (2018) 15-32.

[24] S. Veismoradi, A. Cheraghi, E. Darvishan, Probabilistic mainshock-aftershock collapse risk assessment of buckling restrained braced frames, Soil Dynam. Earthq. Eng. 115 (2018) 205-216.

[25] J. Ruiz-García, E. Bojorquez, E. Corona, Seismic behavior of steel eccentrically braced frames under soft-soil seismic sequences, Soil Dynam. Earthq. Eng. 115 (2018) 119-128.

[26] Y. Liu, X.H. Yu, D.G. Lu, F.Z. Ma, Impact of initial damage path and spectral shape on aftershock collapse fragility of RC frames, Earthq. Struct. 15 (5) (2018) 529-540.

[27] Owen, G. N., & Scholl, R. E. (1981). Earthquake engineering of large underground structures. NASA STI/Recon Technical Report N, 82.

[28] Penzien, J. (2000). Seismically induced racking of tunnel linings. Earthquake engineering & structural dynamics, 29(5), 683-691 .

[29] Hashash, Y. M., Park, D., John, I., & Yao, C. (2005). Ovaling deformations of circular tunnels under seismic loading, an update on seismic design and analysis of underground structures. Tunnelling and Underground Space Technology, 20(5), 435-441 .

[30] Bolouri Bazaz, J., & Besharat, V. (2008, October). An investigation on seismic anakysis of shallow tuneels in soil medium. In 14th World Conference on Earthquake Engineering .

[31] Wang, J. N. (1993). Seismic design of tunnels: a state-of-the-art approach, monograph, monograph 7. Parsons, Brinckerhoff, Quade and Douglas Inc., New York.

[32] Kouretzis, G. P., Sloan, S. W., & Carter, J. P. (2013). Effect of interface friction on tunnel liner internal forces due to seismic S-and P-wave propagation. Soil Dynamics and Earthquake Engineering, 46, 41-51.

[33] Torcato, D. M. M. F. (2010). Seismic behaviour of shallow tunnels in stratified ground. Master's thesis). Univeridade Ténica de Lisboa.

[34] Pakbaz, M. C., & Yareevand, A. (2005). 2-D analysis of circular tunnel against earthquake loading. Tunnelling and Underground Space Technology, 20(5), 411-417 .

[35] Guglielmetti, V., Grasso, P., Mahtab, A., & Xu, S. (Eds.). (2008). Mechanized tunnelling in urban areas: design methodology and construction control. CRC Press.

[36] Wittke, W., Erichsen, C., & Gattermann, J. (2006). Stability Analysis and Design for Mechanized Tunnelling. WBI, Felsbau GmbH, Aachen.